

**Equation of state of hot, dense stellar matter:
Finite temperature
nuclear Thomas-Fermi approach**

Manuel Barranco and Jean-Robert Buchler

Department of Physics and Astronomy, University of Florida, Gainesville, Florida 32611

(Received 23 March 1981)

The properties of hot, dense stellar matter are investigated with a finite temperature nuclear Thomas-Fermi model.

[NUCLEAR STRUCTURE Hot stellar matter, equation of state, finite
temperature nuclear Thomas-Fermi model.]

I. INTRODUCTION

The motivation for the study of matter at densities up to nuclear (i.e., $\rho \leq 0.2 \text{ fm}^{-3} = 3.4 \times 10^{14} \text{ g/cm}^3$) and at temperatures up to several tens of MeV stems from the attempt to model supernova explosions and the possible formation of neutron star remnants. Matter under these astrophysical conditions consists of a mixture of nucleons, some of which may be clustered into nuclei, extreme relativistic, highly degenerate electrons, neutrinos, and photons.

The standard supernova model¹ involves a spherical star of 20 solar masses which has acquired a dense iron core of about 1.5 solar masses, surrounded by an onionlike mantle of successively lighter elements. Most of the mass of the star is in a relatively loosely bound hydrogen envelope. The core has exhausted all its nuclear energy and heats up upon contraction. Finally, iron dissociation into alphas and nucleons causes the adiabatic index $\Gamma_1 = (\partial \ln p / \partial \ln \rho)_s$ to drop below the value of $\frac{4}{3}$, necessary to maintain stable hydrostatic equilibrium. At the onset of collapse typical conditions in the center of the star are $\rho_c \simeq 6 \times 10^9 \text{ g/cm}^3$ and $T_c = 1 \text{ MeV}$ or 10^{10} K . During the collapse the neutrinos are produced by electron captures, and, because of the E^2 dependence of the weak cross sections, become degenerate and are trapped ($\tau_{\text{diffusion}} \gg \tau_{\text{dynamic}}$) at densities in excess of about 10^{12} g/cm^3 , thus preventing further electron captures. As a result, the lepton pressure stays high throughout the collapse and keeps the adiabatic in-

dex close to $\frac{4}{3}$. Core collapse is not halted (core bounce) until the adiabatic index gets sufficiently large again, which occurs when the central density exceeds nuclear matter density (ρ_{NM}). There are two reasons for this stiffening of the equation of state: First, the stiffer nonrelativistic nucleon pressure ($\gamma \sim \frac{5}{3}$) takes over from the extreme relativistic lepton pressure ($\gamma \sim \frac{4}{3}$) when nuclei evanesce near ρ_{NM} . In addition, nuclear forces, which at lower density soften the equation of state, suddenly become very repulsive beyond ρ_{NM} .

When the core bounces, a shock wave forms at the interface between the homologously collapsed core and the infalling mantle. The strength of this shock, which is important if shock ejection of the envelope is to take place, is heavily influenced by the properties of the equation of state during collapse and at bounce, as well as by the neutrino transport out of the core. The neutrino cross sections (particularly for coherent scattering on nuclei) are sensitive to the sizes and abundances of the nuclei which exist at subnuclear densities. Because of their high density of energy levels nuclei have a somewhat larger specific heat,²⁻⁴ C_v , as compared to the degenerate free nucleons. Electron captures and neutrino production are much more efficient on free protons than they are on neutron rich nuclei for which they are blocked because of poor wave function overlap.⁵

It has been suggested that a convectively unstable situation develops after the core bounces because of a negative lepton gradient.^{6,7} Whether this induces a large scale Rayleigh-Taylor overturn of the whole

core on a dynamic timescale with a massive release of trapped neutrinos and concomitant explosion depends again very sensitively on the equation of state.^{7,8} In particular, since the negative lepton gradient at the edge of the neutrino-trapped region is counteracted by a positive entropy gradient, generated by shock heating, cooling by thermal neutrino processes is very important. The latter process occurs most efficiently by weak deexcitation of nuclei, $A^* \rightarrow A + \nu + \bar{\nu}$, and depends extremely sensitively on the nuclear sizes and, of course, on the presence of nuclei.⁹

The nuclear sizes and abundances, as well as the extent of the region of their existence in the (ρ, T) plane, thus have an important bearing on the fate of the core and of the whole star.

The problem we are faced with is to find the most probable arrangement of the nucleons at a given temperature, T , average nucleon density, ρ , and average proton concentration Y_e , with the constraint of charge neutrality. Phrased differently, how do a given number of Z protons, Z electrons, and N neutrons in a given volume V minimize the free energy at a given temperature T . We do not assume beta equilibrium, $e + p \rightleftharpoons n + \nu$, since it does not prevail everywhere during the collapse. The neutrino concentration can then be specified arbitrarily, and since the neutrinos can be treated as a *noninteracting* Fermi gas, they can be omitted in the minimization and added separately to all extensive thermodynamic quantities.

At low densities, low temperatures, and sufficiently large proton concentrations all the nucleons arrange themselves into ironlike nuclei. Towards higher temperatures, dissociation into alpha particles and free nucleons occurs, whereas towards higher densities, neutrons get squeezed out (pressure dissociation). Protons tend to stay clustered as this takes maximum advantage of the nuclear symmetry energy. It is only towards ρ_{NM} that matter becomes a homogeneous mixture of neutrons, protons, and electrons.

In this paper we report on an investigation of the microscopic properties of hot, dense stellar matter making use of a *finite temperature nuclear Thomas-Fermi* (TF) model. This work is based on and is a natural extension of several past studies: (a) the nuclear TF model of Brueckner *et al.*^{10,11} has been very successful in reproducing the bulk properties of zero temperature, terrestrial nuclei; (b) the nuclear TF model has subsequently been successfully applied to the equation of state of zero temperature neutron star matter in beta equilibrium¹²; (c) a finite

temperature extension of the TF model has been used to calculate the level density and specific heat of known terrestrial nuclei² and has shown that the TF model accounts for the experimentally determined specific heat of spherical, nonclosed shell nuclei; (d) phase properties of hot *bulk* matter (i.e., without surface, curvature, nor Coulomb effects) have been studied with the same formalism.¹³ This work has shown that *bulk* nuclear matter has the properties typical of a binary mixture: a line of critical points, a line of equal concentrations, and a line of maximum temperatures. It thus also exhibits the phenomenon of retrograde condensation. A triple point (coexistence of three phases), although possible in principle, has not been found. Although the exact location of these lines is somewhat force dependent, these general features are not.^{13,14} Two-phase bulk matter (TPBM) is a fair first approximation to stellar matter, and its existence boundary also roughly outlines the region of existence of nuclei and some of their gross properties; the high density phase corresponds to the interior of nuclei and tends to always be proton rich, whereas the low density phase corresponds to the internuclear fluid and is essentially devoid of protons.

The advantage of the TF model over a mass formula or liquid drop approach is that it allows the density to vary continuously from the nuclear interior to the external fluid. It also treats fully self-consistently bulk nuclear, surface, curvature, and Coulomb effects. Being a semiclassical approach it is, however, unable to treat shell and pairing effects. Attempts to extend the TF model to deformed nuclei have not been successful. For our purpose here these shortcomings of the TF model are not relevant, however. The astrophysical temperatures of interest wash out shell effects and prevent nuclear deformation. In addition, the large number of degrees of freedom for single particle excitations dwarf the effects of these collective excitations. Furthermore, thermal fluctuations about our typical average nuclear cluster will be seen to be large and will wash out whatever shell and collective effects remain. For these reasons the TF model is ideally suited for the study of the hot, dense matter as occurs during stellar collapse.

Past investigations have used a variety of different approaches, namely a liquid drop model,¹⁴ a finite temperature Hartree-Fock model with a density dependent effective interaction,¹⁵ and, finally, a mass-formula approach together with an *ad hoc* prescription for the nuclear level density.⁴

In Sec. II we shall discuss the energy functional

which underlies both the homogeneous matter and the TF calculations, and we describe the TF model approach. In Sec. III we exhibit the TF results obtained with the Wigner-Seitz approximation and discuss possible improvements due to the inclusion of alpha particles as well as due to finite temperature Coulomb corrections (plasma effects).

II. THE FORMALISM

The nuclear Hamiltonian which we use has only briefly been described elsewhere^{2,13}:

$$H_{\text{nucl}}(\rho_n, \rho_p, \tau_n, \tau_p) = \frac{\hbar^2}{2M}(\tau_n + \tau_p) + V(\rho, \alpha), \quad (1)$$

where

$$\rho = \rho_n + \rho_p, \quad (2)$$

$$\alpha = (\rho_n - \rho_p)/\rho \equiv 1 - 2Y_e, \quad (3)$$

and the kinetic energy is

$$\tau_i = \frac{3}{5}(3\pi^2)^{2/3}\rho_i^{5/3}, \quad i = n, p. \quad (4)$$

The potential energy $V(\rho, \alpha)$ is an interpolation between Lombard's⁹ fit to zero temperature nuclear matter calculations with variable neutron excess V_L valid for $0 \leq \alpha \leq 0.6$, and a pure neutron gas calculation¹⁶ V_N such that

$$V(\rho, \alpha) = (1 - \alpha^2)V_L + \alpha^2V_U, \quad (5)$$

where

$$V_L(\rho, \alpha) = V_1(\rho) + \alpha^2V_2(\rho), \quad (6)$$

$$V_U(\rho, \alpha) = (1 - \alpha^2)V_1 + \alpha^2V_N, \quad (7)$$

$$V_1 = a_1\rho^2 + a_2\rho^{7/3} + a_3\rho^{8/3}, \quad (8)$$

$$V_2 = b_1\rho^2 + b_2\rho^{7/3} + b_3\rho^{8/3}, \quad (9)$$

$$V_N = c_1\rho^2 + c_2\rho^{1.7} + c_3\rho^{2.8}. \quad (10)$$

The coefficients are

$$a_1 = -818.25, \quad b_1 = 258.57, \quad c_1 = -70.9415,$$

$$a_2 = 1371.06, \quad b_2 = 274.21, \quad c_2 = -49.5323,$$

$$a_3 = -556.55, \quad b_3 = -916.08, \quad c_3 = 147.623.$$

The nuclear matter characteristics of this potential are in good agreement with the commonly accepted

ones except for a slightly high value of the nuclear symmetry energy coefficient (about 35 MeV).¹³

As is obvious from the expression of H_{nucl} , the effective mass of our Hamiltonian coincides with the bare mass. That, far from embarrassing, seems to be in good agreement with the most recent estimates which give $M^*/M \gtrsim 1$ near the Fermi surface. Recent systematic calculations of the nuclear specific heat^{2,3} point to $M^* \approx M$ as the best choice for reproducing the experimental results.

We extend the formalism to finite temperature by defining the nuclear free energy density

$$f_{\text{nucl}}(\rho_n, \rho_p, \tau_n, \tau_p, T) = H_{\text{nucl}}(\rho_n, \rho_p, \tau_n, \tau_p) - T(s_n + s_p), \quad (11)$$

with

$$s_i = \frac{5}{6} \frac{\hbar^2}{MT} \tau_i - \eta_i^0 \rho_i \quad (12)$$

and

$$\tau_i = \frac{1}{2\pi^2} \left[\frac{2MT}{\hbar^2} \right]^{5/2} F_{3/2}(\eta_i^0), \quad (13)$$

$$\rho_i = \frac{1}{2\pi^2} \left[\frac{2MT}{\hbar^2} \right]^{3/2} F_{1/2}(\eta_i^0), \quad (14)$$

where

$$F_\nu(z) \equiv \int_0^\infty \frac{x^\nu dx}{e^{x-z} + 1}. \quad (15)$$

The chemical potentials are given by

$$\mu_i = T\eta_i^0 + \frac{\partial V}{\partial \rho_i}. \quad (16)$$

We note that this formulation, which is closer to the finite temperature Hartree-Fock formalism, is actually identical to the one used by Buchler and Epstein,² namely,

$$f_{\text{nucl}}(\rho_n, \rho_p, \tau_n, \tau_p, T) = f_{\text{NI}}(\rho_n, T) + f_{\text{NI}}(\rho_p, T) + V(\rho, \alpha), \quad (17)$$

where f_{NI} is the free energy of a noninteracting fermion gas. The only difference with Refs. 14 and 17 comes from their use of a different nuclear interaction (the Skyrme effective interaction which, when used in its original form,¹⁴ is known to be too repulsive at high density) and, in particular, their use of an effective mass different from the bare mass.

When in the spirit of the TF model we add density gradient terms to the nuclear Hamiltonian to take into account density inhomogeneity corrections and we include the electrons together with the Coulomb energy, we obtain the free energy functional

$$F[\rho_n(r), \rho_p(r), \rho_e(r)] = \int dr^3 (f_{\text{nucl}}[\rho_n(r), \rho_p(r)] + \frac{\hbar^2}{2M} \xi \{ [\nabla(\rho_n + \rho_p)]^2 + \theta [\nabla(\rho_n - \rho_p)]^2 \} + \frac{e}{2} (\rho_p - \rho_e) \Phi_{\text{Coul}}(r) - \frac{3}{4} \left[\frac{3}{\pi} \right]^{1/3} e^2 \rho_p^{4/3} + f_e(\rho_e)). \quad (18)$$

The quantities ξ and θ in front of the gradient terms are, in principle, density and possibly temperature dependent; we have chosen them to be *constants* and have determined them so as to give a good fit to the bulk properties of a large number of known nuclei at zero temperature. ($\xi = 11.4$ and $\theta = -1.2$).

The extreme relativistic, degenerate electrons form an essentially *uniform* negative neutralizing background charge. In the minimization of the free energy density (at given average nucleon density, average proton to nucleon ratio, and temperature) the electron free energy decouples from the equations involving the nucleons. The contribution of the electrons, similarly to that of the neutrinos, can simply be added at the end of the calculation.

Under the conditions of interest here the nucleons can congregate into nuclei embedded in a lower density nucleon fluid or into bubbles in a higher density fluid.^{14,15,18} Both types of configuration will be referred to as nuclear *clusters*. In order to keep the computational complexity manageable we shall assume that we can describe the systems by a typical *average* spherical cluster.

In the spirit of the Wigner-Seitz model we assume that the elemental cluster occupies a spherical cell of volume V_c and radius R_c in which the positive proton charge is neutralized on the average by the electron charge. This charge neutrality guarantees that neighboring cells do not interact and we can reduce the problem to that of a collection of noninteracting spherical cells. The integration in Eq. (18) is carried out over an elemental cell and the average free energy density is $\bar{f} = F_c/V_c$, where F_c is the total free energy [Eq. (18)] extended over a cell. The proton and neutron content of the cell are

$$Z = \int_0^{R_c} \rho_p(r) dr^3 = V_c \rho_e = V_c \rho Y_e, \quad (19)$$

$$N = \int_0^{R_c} \rho_n(r) dr^3 = V_c \rho (1 - Y_e). \quad (20)$$

Instead of minimizing the free energy density through solving the Euler-Lagrange differential equations associated with the functional (18) we have opted for a trial function approach with a Wood-Saxon shape

$$\rho_i(r) = \rho_{1i} + \rho_{2i} \frac{1}{e^{(r-R_i)/a_i} + 1}, \quad i = n, p. \quad (21)$$

The constraints (19) and (20) reduce the number of parameters to six. These functional forms are fairly flexible and have been found to give a good description of the gross properties of terrestrial nuclei.⁸

The constants ρ_{1i} have been added here to account for an external nonvanishing nucleon fluid at the cell boundary. In the case of nuclei (bubbles) the density at the cell center is larger (smaller) than the corresponding cell edge density.

III. BULK MATTER

Bulk matter is defined as homogeneous, but multiphase matter, in which Coulomb and other finite size effects, such as surface energy, are omitted. Bulk matter can serve as a reasonable first approximation to real matter. In Ref. 13 (part of which is hereafter referred to as paper I) we studied the phase properties of nuclear matter (neutrons and protons) as a function of T , ρ , and Y_e . *Single phase homogeneous matter* (SPHM) exhibits a wide domain of instability and of metastability. For example, at 4 MeV and $Y_e = 0.25$, metastability exists between $\rho_1 = 1.28 \times 10^{-4}$ and $\rho_2 = 6.5 \times 10^{-3}$ as well as between $\rho_7 = 1.28 \times 10^{-1}$ and $\rho_8 = 1.43 \times 10^{-1}$. (Unless otherwise specified we use nuclear units, i.e., MeV and fm, with $c = k = 1$.) Instability which occurs between ρ_2 and ρ_7 has different causes: Between ρ_2 and $\rho_3 = 7.5 \times 10^{-3}$ as well as between $\rho_5 = 8.15 \times 10^{-2}$ and $\rho_6 = 1.075 \times 10^{-1}$ diffusive instability ($\partial \mu_n / \partial Y_e > 0$) occurs; between ρ_3 and ρ_5 the isothermal compressibility ($\partial p / \partial \rho)_T$ is negative; finally between $\rho_4 = 1.65 \times 10^{-2}$ and ρ_7 nuclear matter is mechanically unstable ($p_{\text{nucl}} < 0$). When the contribution of the extreme relativistic, degenerate electrons is included, the total pressure is positive everywhere; as a result the region of mechanical instability is removed and the high density region of metastability is increased to $\rho_6 \leq \rho \leq \rho_8$. (For higher values of Y_e it is conceivable that a negative total pressure region might survive because of the larger nuclear attraction; since at the densities where this might arise matter of astrophysical interest is strongly neutronized, we have not bothered to search for this possibility.)

These density intervals are, of course, both tem-

perature and Y_e dependent. For example, at 8 MeV and $Y_e = 0.25$ we find that matter is unstable again between ρ_2 and ρ_7 with $\rho_1 = 2.89 \times 10^{-3}$, $\rho_2 = 1.55 \times 10^{-2}$, $\rho_3 = 2.05 \times 10^{-2}$, $\rho_5 = 6.75 \times 10^{-2}$, $\rho_4 = \rho_6 = \rho_7 = 9.8 \times 10^{-2}$, and $\rho_8 = 1.22 \times 10^{-1}$. At this higher temperature no region of negative pressure exists even for SPHM without electrons. The boundary of the region of coexistence of two separate phases is shown in Fig. 1 as a solid line. The critical point is marked by a cross. The cross-hatched region, bounded by the dashed-dotted-dotted line, is the unstable region for SPHM.

In paper I we ignored the possible presence of alpha particles. In this work we include the alphas, treating them as separate, noninteracting (elementary) pointlike particles with a binding energy $B_\alpha = 28.30$ MeV. The concentration of alpha particles will be found to be always such that we can regard them as a classical gas ($M_\alpha kT/2\pi\hbar^2)^{3/2} \gg \rho_\alpha$, where ρ_α is the number density of alphas.

The concentration $X_\alpha = 4\rho_\alpha/\rho$ of alphas in SPHM at a given total nucleon density ρ , total proton concentration Y_e , and temperature T is found by minimizing the free energy with the constraints of baryon conservation and charge conservation:

$$\rho_N + X_\alpha \rho = \rho, \quad (22)$$

$$Y_N \rho_N + \frac{1}{2} X_\alpha \rho = Y_e \rho, \quad (23)$$

where ρ_N and Y_N are the density and proton concentration, respectively, in the nucleon component, which leads to the equation

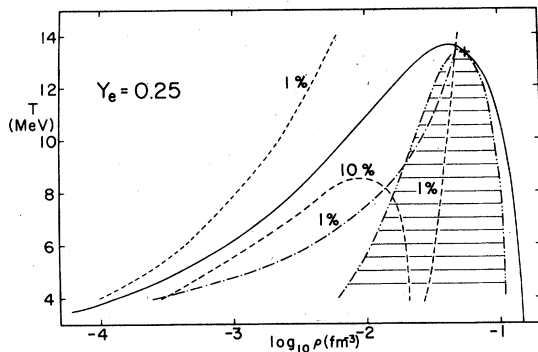


FIG. 1. Phase diagram of nuclear matter and alpha particles in the T - ρ plane. The 1% and 10% alpha-particle concentration lines for (SPHM) are shown dashed. In the region below the two-phase coexistence boundary (solid line) SPHM is unstable and the actual 1% α -concentration line (dashed-dotted) corresponding to two phase matter gets shifted to lower densities.

$$\mu_\alpha(\rho_\alpha, T) = 2\mu_n(\rho_N, Y_N) + 2\mu_p(\rho_N, Y_N), \quad (24)$$

where

$$\mu_\alpha = -kT \ln \left[\left(\frac{M_\alpha kT}{2\pi\hbar^2} \right)^{3/2} / \rho_\alpha \right] - B_\alpha. \quad (25)$$

The α concentration X_α must necessarily lie between 0 and $2Y_e$, where in the latter case all the protons would be absorbed into alpha particles.

The search for alpha particles in TPBM is more complicated. Defining Y_{e1} and Y_{e2} to be the proton concentration in the two phases of the nucleon fluid and ρ_1 and ρ_2 to be the two corresponding nucleon densities, X_α to be the mass fraction of the alphas, and ζ to be the total mass fraction of phase 1 [so that $(1 - \zeta - X_\alpha)$ is the total mass fraction of phase 2] we have the relationships

$$Y_e = \zeta Y_{e1} + (1 - \zeta - X_\alpha) Y_{e2} + \frac{1}{2} X_\alpha, \quad (26)$$

$$\frac{1}{\rho} = \zeta \frac{1}{\rho_1} + (1 - \zeta - X_\alpha) \frac{1}{\rho_2}, \quad (27)$$

together with the equilibrium conditions

$$\mu_n(\rho_1, Y_{e1}, T) = \mu_n(\rho_2, Y_{e2}, T), \quad (28a)$$

$$\mu_p(\rho_1, Y_{e1}, T) = \mu_p(\rho_2, Y_{e2}, T), \quad (28b)$$

$$p(\rho_1, Y_{e1}, T) = p(\rho_2, Y_{e2}, T), \quad (28c)$$

and equation

$$\mu_\alpha(X_\alpha, \rho, T) = 2(\mu_n + \mu_p). \quad (29)$$

It is also clear that μ_α must be the same in both phases. From our neglect of the alpha-nucleon interaction energy it follows that ρ_α is also the same.

The numerical solution of these equations proceeds as follows: We solve Eqs. (28) for ρ_2 , Y_{e1} , and Y_{e2} in terms of ρ_1 at a fixed temperature. Equation (29) is then solved for ρ_α using relation (25). Then we fix Y_e and obtain ρ , ζ , and X_α from the remaining equations, which completes the solution. The solutions for $\zeta = 1$ and $\zeta = 1 - X_\alpha$ define the boundary of the region of the coexistence of two phases. The inclusion of alpha particles causes an inward shift of the existence boundary of TPBM which, however, in Fig. 1 is within the thickness of the line (e.g., at $T = 4$, the left hand boundary gets shifted from $\rho = 1.28 \times 10^{-4}$ to $\rho = 1.26 \times 10^{-4}$).

In Fig. 1 we also show (dashed lines) the $X_\alpha = 1\%$ and 10% concentration lines for SPHM. Obviously SPHM + α is unstable inside the two

phase coexistence region (e.g., all of the 10% line). When breakup into two phases is allowed (TPBM + α) the right hand branch of the $X_\alpha = 1\%$ line shifts to much lower density (dashed-dotted line). We therefore conclude that TPBM + α has a very

low α concentration ($X_\alpha < 10\%$), at least for Y_e in the vicinity of $Y_e = 0.25$. Finite size effects of the α 's are negligible and hardly affect X_α . The variation of X_α with Y_e is difficult to predict in general since

$$\frac{dX_\alpha}{dY_e} = \frac{2}{1 - X_\alpha} \left[\frac{\partial \mu}{\partial Y_N} \right]_{\rho_N} / \left[\frac{kT}{X_\alpha} + 2\rho \left[\frac{\partial \mu}{\partial \rho_N} \right]_{Y_N} + \frac{(1 - 2Y_N)}{(1 - x)^2} \left[\frac{\partial \mu}{\partial Y_N} \right]_{\rho_N} \right], \quad (30)$$

where $\mu \equiv \mu_n + \mu_p$, depends on the derivatives of μ which do not have a definite *sign*.

The results of paper I which omit alphas are thus essentially unchanged. Whether the inclusion of a nuclear interaction between the alpha particles and the nucleons has an appreciable effect on their concentration is under investigation.

IV. THOMAS-FERMI MODEL RESULTS

Preliminary results of the TF model have been summarized elsewhere.¹⁸ We present here a more complete description of the model and more detailed results, as well as an analysis of the sensitivity of the results to the input physics. In the following we first treat the system in the Wigner-Seitz approximation and omit alpha particles. Then successively we introduce finite temperature plasma effects and include alpha particles in our treatment.

As we have mentioned in Sec. II we assume a Wigner-Seitz (WS) model for the configuration of the nucleons with a spherically symmetric cell, and a spherically symmetric arrangement of the nucleons around the cell center. With that constraint it turns out that at low density one obtains a bulge of nucleons in the cell center (*nuclei*), whereas at higher density a nucleon deficiency (*bubble*) occurs, as was noted previously. Both configurations will be referred to as *clusters*. We find that for $Y_e = 0.25$ this transition from nuclei to bubbles occurs at $\rho = 6.3 \times 10^{-2}$ at 4 MeV and at $\rho = 5.2 \times 10^{-2}$ at 8 MeV. As the density is increased the size of the nuclei increases to about $A_{\text{clus}} = 770$ at the nucleus-bubble transition, from which point on the bubble size $A_{\text{clus}} = -1340$ shrinks until the transition to homogeneous matter. When a smoothly varying nucleon distribution is taken into account, as with the TF model, the bubble size is quite naturally defined as the *deficiency* of nucleons with respect to the *outside* (background)

nucleon density, i.e., the density at the cell radius: the same way that the size of the nuclei is defined as the nucleon bulge *above* the background. (This definition differs from that of Lamb *et al.*¹⁴ who consider step-function densities and then define the bubble size as the number of nucleons inside the low density part.)

The results of our calculations at $T = 4$ and 8 MeV are exhibited in Tables I and II, respectively. The nuclei are seen to always be rather large, which is in agreement with both the liquid drop¹⁴ and the finite temperature Hartree-Fock results.¹⁵

The first two columns show the nuclear part of the internal energy and entropy per nucleon (which we define to be the total minus the electrons' contribution). Also shown are the cells' central and boundary densities. The asterisks indicate that the density was so small that we did not deem it worth the effort to pinpoint it. The parameter Γ is indicative of the nature of the plasma and will presently be discussed. The nuclear part of chemical potentials $\langle \mu_n \rangle$ for the neutrons and protons, respectively, have been *estimated* as follows:

$$\langle \mu_i \rangle = \frac{\int_0^{R_c} \mu_i(r) r^2 \rho_i(r) dr}{\int_0^{R_c} r^2 \rho_i(r) dr},$$

where

$$\mu_i = \frac{\partial f_{\text{nucl}}}{\partial \rho_i} - 2\xi \frac{\hbar^2}{2M} \nabla^2 \rho + e\phi(r) \delta_{ip}, \quad i = n, p.$$

A more accurate evaluation as a numerical derivative of the free energy, $\mu_n = \partial \bar{f} / \partial \bar{\rho}_n$, $\mu_p = \partial \bar{f} / \partial \bar{\rho}_p$, would have been too costly. We note that in contrast, the entropy which is the temperature derivative of \bar{f} could be obtained directly at a given temperature because of the form of Eq. (17). For reference we also give the chemical potential of the electrons in the last column. The pressure p has been obtained by differentiation with respect to ρ of a

TABLE I. Thomas-Fermi results for nuclear clusters (nuclei or bubbles) at $T = 4$ MeV and $Y_e = 0.25$ using the Wigner-Seitz approximation (see text for explanation). Asterisks mean that the missing quantity was not calculated with meaningful accuracy.

ρ	E/A	S/kA	R_c	$\rho_n(0)$	$\rho_p(0)$	$\rho_n(R_c)$	$\rho_p(R_c)$	A	A_{clus}	Z_{clus}	Γ	$\langle \mu_n \rangle$	$\langle \mu_p \rangle$	μ_e
0.005	-3.32	1.65	20.1	8.64(-2)	5.47(-2)	1.64(-3)	*	170	114	42	32	-3.90	-22.0	65.0
0.010	-4.00	1.32	17.0	8.93(-2)	5.10(-2)	2.75(-3)	*	206	149	51	56	-1.93	-26.2	82.2
0.020	-4.60	1.06	16.9	9.18(-2)	4.72(-2)	4.47(-3)	*	276	214	69	115	-.05	-30.8	103.9
0.025	-4.79	0.99	14.4	9.24(-2)	4.56(-2)	5.15(-3)	*	313	248	78	153	.56	-32.5	112.0
0.030	-4.93	0.94	14.2	9.28(-2)	4.44(-2)	5.83(-3)	*	359	290	90	205	1.01	-33.8	119.0
0.040	-5.18	0.86	14.1	9.31(-2)	4.23(-2)	7.11(-3)	*	468	385	117	350	1.76	-36.0	131.1
0.050	-5.37	0.81	14.3	9.30(-2)	4.03(-2)	8.30(-3)	*	617	576	154	598	2.34	-37.9	141.3
0.060	-5.53	0.76	14.9	9.29(-2)	3.88(-2)	9.98(-3)	*	840	703	210	1061	2.84	-39.4	150.2
0.070	-5.70	0.73	16.0	9.64(-3)	*	8.73(-2)	3.48(-2)	1192	-892	-250	1963	4.48	-49.9	158.2
0.080	-5.90	0.70	14.8	1.08(-2)	*	8.82(-2)	3.39(-2)	1078	-577	-188	865	4.60	-50.6	165.4
0.090	-6.07	0.68	13.9	1.19(-2)	*	8.91(-2)	3.30(-2)	1014	-365	-119	367	4.67	-51.3	172.0
0.100	-6.20	0.65	13.6	1.43(-2)	*	8.81(-2)	3.14(-2)	1058	-207	-68	123	4.74	-51.9	178.2
0.105	-6.28	0.65	14.5	1.44(-2)	*	8.65(-2)	3.00(-2)	1331	-146	-47	55	*	*	181.1
0.107	-6.30	0.65	15.5	1.50(-2)	*	8.44(-2)	2.88(-2)	1669	-97	-31	23	*	*	182.3

spline function fitted to the free energy per baryon at constant T and Y_e , $p = \rho^2 [\partial(F/A) / \partial \rho]_{Y_e, T}$. The ionic radius R_c is found to vary very little. Its odd behavior in the vicinity of the nucleon-bubble phase transition is probably not physical, but an artifact of our constraint of sphericity in the basic cell which breaks down when the cluster radius becomes a sizable fraction of the cell radius. This problem is germane to any approach based on the Wigner-Seitz model.

We have assumed here that we can replace the actual nuclear cell distribution by a *typical* average cell as is also done elsewhere.^{14,15} Near the critical point ($\rho = 5.62 \times 10^{-2} \text{ fm}^{-3}$ and $T = 13.30$ MeV for $Y_e = 0.25$) fluctuations are expected to be very large. Actually, even far away from the critical

point such cell fluctuations are surprisingly large; as a measure of the fluctuations we exhibit in Table III the quantity

$$P(R_c) = P(R_c^*) e^{[F(R_c^*) - F(R_c)]/kT}, \quad (31)$$

where R_c^* is the most probable cell radius for a given $\rho = 0.04$ and $Y_e = 0.25$ at 4 and 8 MeV temperature.

TF nucleon density distributions have been exhibited in Ref. 16 (hereafter referred to as paper II) for various nucleon densities and for the favored arrangement (nucleus or bubble) at 4 MeV and $Y_e = 0.25$. Here we show in Fig. 2 the variations of the nucleon distributions with temperature, for a nucleus case ($\rho = 0.03$) and for a bubble case

TABLE II. Thomas-Fermi results for nuclear clusters (nuclei or bubbles) at $T = 4$ MeV and $Y_e = 0.25$ using the Wigner-Seitz approximation (see text for explanation). Asterisks mean that the missing quantity was not calculated with meaningful accuracy.

ρ	E/A	S/kA	R_c	$\rho_n(0)$	$\rho_p(0)$	$\rho_n(R_c)$	$\rho_p(R_c)$	A	A_{clus}	Z_{clus}	Γ	$\langle \mu_n \rangle$	$\langle \mu_p \rangle$	μ_e
0.025	0.99	1.94	13.1	7.78(-2)	4.25(-2)	8.89(-3)	*	236	143	50	35	-4.59	-33.6	110.6
0.03	0.46	1.83	12.9	7.84(-2)	4.09(-2)	9.91(-3)	*	269	172	59	49	-3.77	-35.3	117.7
0.04	-0.31	1.67	12.8	7.89(-2)	3.79(-2)	1.17(-2)	*	355	245	82	93	-2.48	-38.2	129.9
0.05	-0.82	1.56	13.3	7.91(-2)	3.55(-2)	1.41(-2)	*	487	344	113	175	-1.48	-40.6	140.2
0.06	-1.15	1.49	14.9	1.44(-2)	*	6.97(-2)	2.87(-2)	836	-546	-194	313	1.06	-50.4	149.1
0.08	-1.96	1.36	12.7	1.71(-2)	*	7.24(-2)	2.67(-2)	690	-167	-58	33	1.13	-51.4	164.4

TABLE III. Relative probability of cell fluctuations at a density of 0.04 fm^{-3} , temperature of 4 MeV and $Y_e = 0.25$.

$T = 4 \text{ MeV}$		$T = 8 \text{ MeV}$	
R_c	$P(R_c)/P(R_c^{eq})$	R_c	$P(R_c)/P(R_c^{eq})$
8	0.8940	11	0.9974
14	0.9978	12	0.9995
14.08	1.0000	12.84	1.0000
15	0.9984	13	0.9999
16	0.9937	14	0.9991
17	0.9866	15	0.9970
18	0.9775		
19	0.9668		
25	0.8873		

($\rho = 0.08$). Essentially all the protons are associated with the denser phase, i.e., with the nuclei at low density and with the "shell" surrounding the bubble at higher density. This arrangement takes maximum advantage of the isospin zero nuclear attraction and was already noted for TPBM. Thermal effects cause the nucleons to spread out more as is evidenced in Fig. 2, which shows both a nucleus and a bubble configuration at a temperature of 4 and 8 MeV.

In Fig. 3 we show the variation of the shape of the nucleon distributions with Y_e . It is not astonishing that the central neutron density increases and the central proton density decreases with increasing

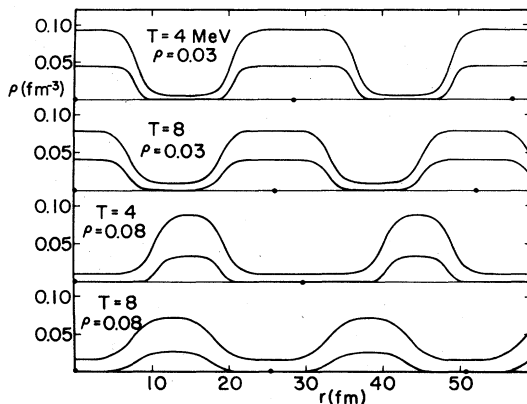


FIG. 2. Variation with temperature of the spatial neutron (upper) and proton (lower curve) distribution in the case of nucleus configuration (upper two figures) and a bubble configuration (bottom two figures). The dots on the axis correspond to cell centers.

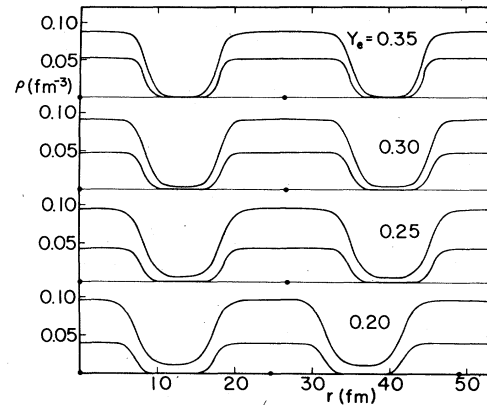


FIG. 3. Variation with proton concentration of the nucleon distributions at a temperature of 4 MeV (see also Fig. 2).

neutron excess, while at the same time the outside neutron density increases. While the cell radius stays more or less constant down to $Y_e = 0.25$, below that value the nuclei begin to shrink, as is evidenced by the $Y_e = 0.2$ case.

Figure 4 shows the free energy per nucleon (inclusive of the electron contribution) as a function of density at two temperatures, 4 and 8 MeV, and a proton concentration of $Y_e = 0.25$. The dashed line corresponds to SPHM and the arrow denotes the

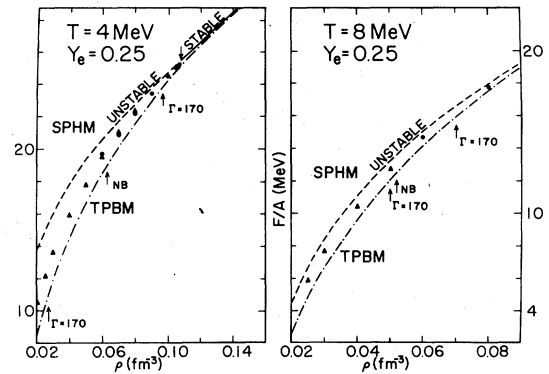


FIG. 4. Free energy (inclusive of electrons) per nucleon as a function of density. The dashed line corresponds to single phase homogeneous matter and its stability is indicated. The dashed-dotted line refers to two-phase bulk matter. The triangles correspond to the TF nucleus solutions and the circles correspond to the TF bubble solutions. The nucleus bubble (NB) transition is indicated by an arrow. The Coulomb phase transitions are indicated by $\Gamma = 170$.

stability boundary. The dashed-dotted line, which necessarily lies below, corresponds to TPBM. The TF-nucleus solutions are indicated by triangles and the TF-bubble solutions by full circles. The transition from nuclei to bubbles (NB) is marked with an arrow.

The precise location of the (physical) phase transition from clustered matter (bubbles) to SPHM presents numerical difficulties. The reason is that in the evaluation of the free energy of a cell [Eq. (18)] the bubble region contributes less and less as the transition is approached because of the $4\pi r^2$ weighing factor. However, since the combined effects of surface, curvature, and Coulomb energy are always positive, the free energy of clustered matter always lies above that of TPBM and thus disappears *before* $\rho = \rho_8$, which is the maximum density at which TPBM can exist. (We have seen that α particles hardly affect this density). On the other hand, SPHM becomes unstable below $\rho = \rho_6$ and can be metastable above. The transition from clustered matter to SPHM must therefore occur for $\rho_6 < \rho < \rho_8$. A similar argument shows that at lower density the nuclei must disappear (dissociate) for $\rho_1 < \rho < \rho_2$. This conclusion is at variance with the results of Ref. 14, which finds no such boundary for the disappearance of the nuclei towards lower density. The discrepancy could be due to the

effects of the translational free energy of the clusters.¹⁹ Our energy functional gives rise to a TPBM coexistence boundary which lies at considerably lower temperatures¹³ than that of Ref. 14, e.g., with $Y_e = 0.5$, our $T_{\max} = 15.5$ MeV, versus their $T_{\max} = 20.2$ MeV. Since the existence boundary of nuclei or bubbles lies below the corresponding boundary for TPBM, it is to be expected that our clusters also dissociate at correspondingly lower temperatures.

Two Coulomb phase transitions can exist in stellar matter. One occurs for the nucleus configuration from a Coulomb liquid to a Coulomb crystal. To the extent that we can approximate the nuclei by point charges in a neutralizing background of electrons and "external" protons, a phase transition occurs when $\Gamma \equiv Z_{\text{eff}}^2 e^2 / kTR_c$ exceeds about 170,²⁰ where $Z_{\text{eff}} = Z_{\text{clus}}$. Similarly, a phase transition can occur from a Coulomb solid of bubbles to a bubble liquid again when Γ decreases through 170 with increasing density. Now Z_{eff} is negative since the bubbles are a charge deficiency as compared to the external (high density) proton charge minus the uniform negative electron background. The locations of the two transitions are marked with an arrow in Fig. 4.

Figure 5 exhibits the equations of state at two temperatures, 4 and 8 MeV, for a proton concentra-

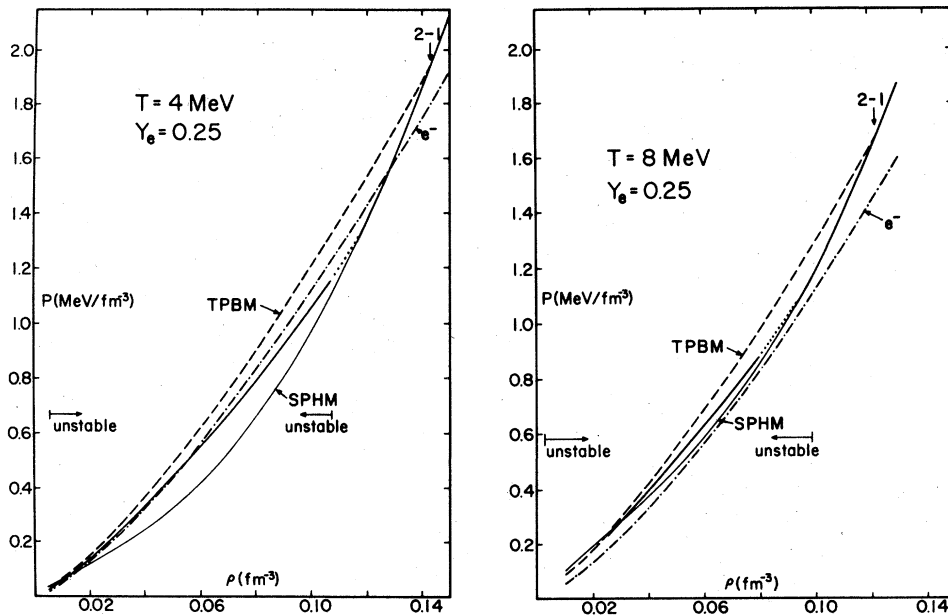


FIG. 5. Equations of state at temperatures of 4 and 8 MeV for strongly phase homogeneous matter (SPHM, solid line), two phase bulk matter (TPBM, dashed line). The TF pressure, shown as a thick solid line, merges into SPHM above a certain transition density (the dotted line is an extrapolation). The thick line thus corresponds to the physical equation of state. For reference the electron pressure is also shown (dashed-dotted).

TABLE IV. Same as Table I but including plasma effects. The last entry is the plasma free energy divided by the nuclear free energy.

ρ	E/A	S/kA	R_c	$\rho_n(0)$	$\rho_p(0)$	$\rho_n(R_c)$	$\rho_p(R_c)$
0.005	-3.08	1.67	15.8	8.42(-2)	5.46(-2)	1.61(-3)	*
0.02	-4.53	1.07	13.2	9.22(-2)	4.81(-2)	4.37(-3)	*
0.03	-4.90	0.95	13.0	9.33(-2)	4.53(-2)	5.74(-3)	*
0.04	-5.16	0.86	13.3	9.39(-2)	4.31(-2)	6.97(-3)	*

tion $Y_e = 0.25$. The line marked SPHM corresponds to single phase homogeneous matter and its region of instability is indicated. The dashed line corresponds to TPBM and the transition from TPBM to SPBM is indicated by an arrow (2-1). For reference we also indicate the pressure of the electron component. The actual equation of state, obtained with the TF model, is shown as a thick solid line. As mentioned above, numerical difficulties preclude the exact delineation of the phase transition to SPHM (the dotted line is an *ad hoc* extrapolation). We can now quantify the earlier statement that TPBM is a reasonable approximation to actual matter; the difference is seen to be of the order of or less than a factor of 2.

Our formalism so far has included plasma effects only in the strongly coupled limit (Wigner-Seitz approximation) which corresponds to a dense, cold plasma, although we have included thermal dilatation of the nucleon distributions in our free energy [Eq. (18)]. We discuss now an attempt to improve upon this approximation and include other finite temperature effects in the following way: We include a plasma energy term of the form

$$F_{pl} = F_0(\rho_c, T) + (F_{cx} - 0.89\Gamma\rho_c kT), \quad (32)$$

where $\rho_c = 1/V_c$ is the number density of cells and where we have subtracted the Wigner-Seitz term for point particles since the latter energy is already included in Eq. (18) and actually takes some finite size effects into account. For the so-called Coulomb-excess free energy F_{cx} we have used a fitting formula to Monte Carlo results both for the liquid and for the solid.²⁰ The noninteracting free energy F_0 , which is defined to be the classical particle translational energy for point particles for the liquid phase, is given by

$$F_0 = -\rho_c kT \ln \left[\left(\frac{A_{\text{eff}} M k T}{2\pi \hbar^2} \right)^{3/2} \frac{e}{\rho_c} \right], \quad (33)$$

and the Debye oscillator expression in the case of a solid. We have approximated A_{eff} by A_{clus} , i.e., we assume that the nucleon bulge behaves like a free classical particle. $F_{cx}(\Gamma, \xi)$ customarily is defined to depend on the packing fraction $\xi = (R_{\text{clus}}/R_c)^3$ and thus to include finite size effects, i.e., both the excluded volume and the reduced Coulomb repulsion. In principle, F_{pl} has to be included in the full minimization in order to treat it self-consistently. However, in practice we have found that the results of $F_{WS}(R_c)$ with the Wigner-Seitz model can be used to evaluate $F_{pl}(R_c)$ and that the minimum of $R_{WS}(R_c) + F_{pl}(R_c)$ is very close to the self-consistent one.

We have tested the sensitivity of the results to the packing fraction ξ by including only the excluded volume part of the translational free energy. This has caused a very small shift towards smaller nuclei.

In Table IV we show the results of our inclusion of F_{pl} at 4 MeV for the nucleus configuration where, however, we have neglected the packing fraction ($\xi = 0$). Comparison with Table II shows a marked decrease of the cluster sizes, by a factor of 2 or more at low density, although the additional plasma energy F_{pl} is a small fraction of the total free energy (excluding the electron contribution). At higher temperatures we have encountered difficulties with F_{pl} . The TF solution (cluster) disappears, i.e., one can obtain the homogeneous SPHM solution in a density region where the latter is unstable. We believe that this difficulty arises from an inconsistency in the physical description: On the one hand, the nuclear energy is treated in a Wigner-Seitz cell method without allowing for size and shape fluctuations, and on the other hand, one superposes on this a finite temperature plasma description of a classical system of mobile charged spheres. However, it is difficult to see how one could improve upon this physical description. We should point out that our TF model is not the only one encountering this dif-

TABLE IV. (Continued).

A	A_{clus}	Z_{clus}	Γ	$\langle \mu_n \rangle$	$\langle \mu_p \rangle$	μ_e	$F_{\text{pl}}/F_{\text{tot}}^{\text{nucl}}$
83	56	20	10	-3.87	-23.1	65.0	4.3(-2)
191	149	48	62	-5.47	-31.4	103.9	1.6(-2)
278	225	69	133	0.99	-34.1	119.0	9.7(-3)
395	326	99	264	1.75	-36.2	131.1	6.4(-3)

difficulty; the latter must also arise overtly or covertly in any approach based on a Wigner-Seitz cell description.

Since the disappearance of the TF cluster solution occurs through a shrinking of the cluster size we have also included alpha particles in the TF model in an attempt to resolve the difficulty of not finding a solution other than the SPHM solution, where the latter is unstable. We have treated the Coulomb energy of the mixture of nuclear clusters and alphas in a linear combination approximation as suggested by Hansen *et al.*²¹ The inclusion of alphas increases the numerical expense of obtaining a solution of the TF equation. We find, however, that the concentration of alphas is again very small, similar to that in the case of TPBM + α (e.g., at $\rho = 0.005$, $T = 4$ MeV, $Y_e = 0.25$ one obtains $X_\alpha = 0.016$). For comparison purposes, at $\rho = 0.005$, $Y_e = 0.25$, $T = 4$ MeV the total free energies (inclusive of the electrons) are $F_{\text{WS}}/A = 2.13$ MeV, $F_{\text{WS+pl}}/A = 1.85$ MeV, and $F_{\text{WS+pl}+\alpha}/A = 1.83$ MeV. The inclusion of alphas does not seem to resolve the above mentioned difficulty. A consistent treatment of the nuclear and plasma physics at high temperatures requires further attention.

V. CONCLUSIONS

The nuclear Thomas-Fermi model with a Wigner-Seitz approximation has been shown to lend

itself naturally to the study of the clustering of nucleons in hot, dense matter. Together with the finite temperature Hartree-Fock approach,¹⁵ most useful at low temperatures, it is the only model which treats nuclear bulk, surface, curvature, and (Wigner-Seitz) Coulomb effects fully selfconsistently.

Our study of the equation of state of dense, hot matter shows that the thermodynamic variables, like energy and pressure, are fairly insensitive to the exact arrangement of the nucleons. The sizes of the nuclear clusters (nuclei or bubbles), on the other hand, are found to exhibit an uncomfortable sensitivity to relatively small effects, like the temperature dependence of the Coulomb energy and the kinetic energy associated with the motion of the clusters.

ACKNOWLEDGMENTS

It is a pleasure to acknowledge fruitful discussions with many colleagues during the development of the series of papers devoted to the equation of state of hot, dense matter. We would specially like to thank R. Coldwell, J. M. Lattimer, R. J. Lombard, J. P. Hansen, J. Treiner, P. Vieillefosse, X. Viñas, and D. Vauterin. This work has been supported by the National Science Foundation (Grant AST79-20024) and by the Northeast Regional Data Center at the University of Florida.

¹For an excellent recent review, see J. C. Wheeler, Rep. Phys. (in press).

²J. R. Buchler and R. J. Epstein, *Astrophys. J. Lett.* **235**, 91 (1980).

³M. Barranco and J. Treiner, *Nucl. Phys.* **A351**, 269 (1981).

⁴T. J. Mazurek, J. M. Lattimer, and G. E. Brown, *Astrophys. J.* **229**, 713 (1979); M. F. El Eid and W. Hillebrandt, *Astron. Astrophys. Suppl. Ser.* **42**, 215 (1980).

⁵G. Fuller, W. A. Fowler, and M. Newman, *Astrophys. J. Suppl. Ser.* **42**, 447 (1980); see also H. A. Bethe, G. E. Brown, J. Applegate, and J. M. Lattimer, *Nucl. Phys.* **A324**, 487 (1979).

⁶R. I. Epstein, *Mon. Not. R. Astron. Soc.* **188**, 305 (1979); S. A. Colgate and A. G. Petschek, *Astrophys. J. Lett.* **236**, L115 (1980); M. Livio, J. R. Buchler, and S. A. Colgate, *Astrophys. J. Lett.* **238**, L139 (1980).

⁷J. R. Buchler, M. Livio, and S. A. Colgate, *Proceedings of the 58th Colloquium of the International Astronomical Union* (unpublished).

⁸J. M. Lattimer, and T. J. Mazurek *Astrophys. J.* (in press).

⁹E. W. Kolb and T. J. Mazurek, *Astrophys. J.* **234**, 1085 (1979).

¹⁰K. A. Brueckner, J. R. Buchler, S. Jorna, and R. J. Lombard, *Phys. Rev.* **171**, 1188 (1968); K. A.

- Brueckner, J. R. Buchler, R. C. Clark, and R. J. Lombard, *Phys. Rev.* 181, 1543 (1969).
- ¹¹R. J. Lombard, *Ann. Phys. (N.Y.)* 77, 380 (1973).
- ¹²J. R. Buchler and Z. Barkat, *Astrophys. Lett.* 7, 167 (1971); J. R. Buchler and Z. Barkat, *Phys. Rev. Lett.* 27, 48 (1971); Z. K. Barkat, J. R. Buchler, and L. Ingber, *Astrophys. J.* 176, 723 (1972).
- ¹³J. R. Buchler and M. Barranco, *J. Phys. (Paris) Coll. C2*, 31 (1980); M. Barranco and J. R. Buchler, *Phys. Rev. C* 22, 1729 (1980), referred to as paper I; X. Viñas, J. Garcia-Roger, and M. Barranco, *Phys. Lett. B100*, 209 (1981).
- ¹⁴D. Q. Lamb, J. M. Lattimer, C. J. Pethick, and D. G. Ravenhall, *Phys. Rev. Lett.* 41, 1623 (1978).
- ¹⁵P. Bonche and D. Vautherin, *Nucl. Phys.* (to be published).
- ¹⁶J. R. Buchler and L. Ingber, *Nucl. Phys.* A170, 1 (1971).
- ¹⁷J. M. Lattimer and D. G. Ravenhall, *Astrophys. J.* 223, 314 (1978); D. Q. Lamb, J. M. Lattimer, C. J. Pethick, and D. G. Ravenhall, *Nucl. Phys.* A360, 459 (1981).
- ¹⁸M. Barranco and J. R. Buchler, *Astrophys. J. Lett.*, 245, L109 (1981), referred to as paper II.
- ¹⁹J. M. Lattimer (private communication).
- ²⁰W. L. Slattery, G. D. Doolen, and H. E. DeWitt, *Phys. Rev. A* 21, 2087 (1980).
- ²¹J. P. Hansen, G. M. Torrie, and P. Vieillefosse, *Phys. Rev. A* 16, 2153 (1977); B. Brami, J. P. Hansen, and F. Joly, *Physica* 95A, 505 (1979).